A multi-temporal and multi-angular approach for systematically retrieving soil moisture and vegetation optical depth from SMOS data

Yu Bai[a,b], Tianjie Zhao[a†], Li Jia[a†], Michael H. Cosh[c], Jiancheng Shi[d], Zhiqing Peng[a,b], Xiaojun Li[e], Jean-Pierre Wigneron[e]

[a] State Key Laboratory of Remote Sensing Science, Aerospace Information Research Institute, Chinese Academy of Sciences, China
[b] University of Chinese Academy of Sciences, China
[c] USDA-ARS Hydrology and Remote Sensing Laboratory, United States of America
[d] National Space Science Center, Chinese Academy of Sciences, China
[e] INRAE, UMR1391 ISPA, F-33140, Villenave d'Ornon, France

†Corresponding authors: T. Zhao; L. Jia (mail to: zhaotj@aircas.ac.cn; jiali@aircas.ac.cn)

1. Introduction

Surface soil moisture (SM) usually refers to the soil moisture in the upper soil layer of 0-5 cm, and plays a key role in governing the exchanges of water and energy between the land and the atmosphere. Currently, microwave L-band radiometer is considered an appropriate tool for spatial SM mapping from space due to its strong penetration of vegetation covers and sensitivity to surface SM conditions (Kerr et al., 2001). Launched by the ESA in 2009, SMOS (Soil Moisture and Ocean Salinity) was the first satellite to operate with a L-band (1.4 GHz) radiometer and had provided more than 10 years of observation data. However, there are some problems in the current SMOS soil moisture retrieval algorithm, including ignoring the polarization difference of microwave radiation in vegetation layer, the error accumulation of retrievals caused by iterative algorithms, and the uncertainty of retrievals caused by some static auxiliary parameters (such as soil roughness and effective scattering albedo) used in the algorithm, which indicates that the performance of existing SMOS soil moisture products could still be improved. Microwave retrieval of soil moisture is an underdetermined problem, as microwave emission from the landscape is affected by a variety of surface parameters. Increasing observation information is an effective means to make retrievals more robust. Therefore, this study proposes a multi-temporal and multi-angular (MTMA) approach to systematically retrieve the four parameters of vegetation optical depth (VOD_p, p indicates the polarization (H: horizontal, or V: vertical)), effective scattering albedo (ω_p^{eff}), soil surface roughness (Z_p^S), and soil moisture (SM_p) using SMOS L-band data, in order to improve the performance of soil moisture retrieval and provide higher quality soil moisture products for the applications of land surface process models, hydrological models and agricultural monitoring, etc.

2. Method

Since the observed microwave radiation of land surfaces are the composition of vegetation and soil emissions, the major challenge for accurate retrieval of SM is to decouple the soil and vegetation contributions, which is also the main difference between current retrieval algorithms. One of the approaches for decoupling soil-vegetation effects is the use of MVIs (Shi et al., 2008; 2019), which minimize the soil contribution and can be used for deriving vegetation contributions independently without any inputs regarding to soil parameters. This MVIs approach has been demonstrated by a previous study (Cui et al., 2015) only using the H-pol brightness temperature (TB) with a priory information of ω_p^{eff} based on land cover types. In this study, we further introduce the multi-temporal information to retrieve both VOD_p and ω_p^{eff}, which are expected to be a more accurate estimation of vegetation effects. The retrieved VOD_p and ω_p^{eff} are then used for retrieving soil emissivity (related to SM and soil roughness).

2.1 Retrieval of vegetation parameter

Combining the $\tau-\omega$ model and a linear relationship between the soil emissivity at two incidence angles (Shi et al., 2019), the linear relationship between the TB at two incidence angles is obtained and the soil information (such as E_p^S) is removed as below:

$$TB_p(\theta_2) = \alpha_p(\theta_1,\theta_2)\cdot V_p^a(\theta_2) + V_p^e(\theta_2) - \beta_p(\theta_1,\theta_2)\cdot \frac{V_p^a(\theta_2)}{V_p^a(\theta_1)}\cdot V_p^e(\theta_1) + \beta_p(\theta_1,\theta_2)\cdot \frac{V_p^a(\theta_2)}{V_p^a(\theta_1)}\cdot TB_p(\theta_1) \quad (1)$$

where V_p^e and V_p^a are vegetation emission term and attenuation term respectively, and written as

$$V_p^e(\theta) = \left(1-\Gamma_p(\theta)\right)\cdot\left(1-\omega_p\right)\cdot\left(1+\Gamma_p(\theta)\right)\cdot T^c \quad (2)$$

$$V_p^a(\theta) = \Gamma_p(\theta)\cdot T^s - \left(1-\Gamma_p(\theta)\right)\cdot\left(1-\omega_p\right)\cdot\Gamma_p(\theta)\cdot T^c \quad (3)$$

where T^c (K) and T^s (K) are the canopy and soil temperature respectively, and are assumed to be equal and expressed by the effective soil temperature (T^{eff}); Γ_p is the vegetation transmissivity $\left(\Gamma_p = exp(-\tau_p^c / cos(\theta))\right)$; τ_p^c means the VOD_p; ω_p^{eff} is the vegetation effective scattering albedo; The coefficients of $\alpha_p(\theta_1,\theta_2)$ and $\beta_p(\theta_1,\theta_2)$ are obtained by constructing the linear relationship between soil emissivity at two incident angles using the simulated dataset by the AIEM. The unknowns in Eq. 1-3 include two vegetation parameters (VOD_p and ω_p^{eff}). In this study, the SMOS H-pol TB in three angle pairs (i.e. (30°, 40°), (35°, 45°) and (40°, 50°)) or SMOS V-pol TB in three angle pairs (i.e. (15°, 30°), (20°, 35°) and (25°, 40°)) are used for retrievals of VOD_p and ω_p^{eff}.

In this study, the multi-temporal approach is further introduced to include more information to enable the simultaneous retrieval of VOD_p and ω_p^{eff}, which assumes that the vegetation attributes are almost unchanged over a short period, that is, they are set as constants (at several temporal adjacent overpasses) (Konings et al., 2016, 2017). VOD_p and ω_p^{eff} will be resolved simultaneously when the cost function (Eq. 4) is minimum:

$$\min_{X=VOD_p,\ \omega_p^{eff}} COST_p^{vegetation}(X) = \sum_{t=1}^{N}\sum_{i=1}^{K}\left[TB_p{}^t(\theta_i) - TB_p^{o\,t}(\theta_i)\right]^2 / \sigma\left(TB_p^o\right)^2 \quad (4)$$

where t is the overpassing time of the SMOS satellite, σ is the standard deviation of SMOS observed TB, N is the number of satellite overpassing time, K is the number of observation angle pairs, $TB_p(\theta)$ is simulated TB, $TB_p^o(\theta)$ is SMOS observed TB, X (VOD_p and ω_p^{eff}) is the parameter to be retrieved.

2.2 Retrieval of soil parameter

After retrieving the vegetation parameters, the rough soil emissivity could be simulated, with the SM_p and Z_p^S remaining to be unknowns. The SM_p and Z_p^S can be retrieved using a parametric soil emissivity model (Eq. 5) developed by Zhao et al. (2015):

$$E_p^S(\theta) = \left(1 - r_p^S(\theta)\right)\cdot\left[A_p\cdot exp\left(B_p\cdot Z_p^{S\,2} + C_p\cdot Z_p^S\right)\right] \quad (5)$$

where Z_p^S (cm) is the soil roughness slope parameter; A_p, B_p and C_p are regression coefficients.

When auxiliary data (surface effective temperature, soil texture) are obtained, SM_p and Z_p^S can be retrieved when the cost function (Eq. 6) is minimum:

$$\min_{X=SM_p,\ Z_p^S} COST_p^{soil}(X) = \sum_{t=1}^{N}\sum_{i=1}^{K}\left[E_p{}^t(\theta_i) - E_p^{o\,t}(\theta_i)\right]^2 \quad (6)$$

where $E_p{}^t(\theta)$ is the simulated soil emissivity at the overpassing time t, $E_p^{o\,t}(\theta)$ is soil emissivity calculated from observed TB of SMOS with retrieved vegetation parameters at the overpassing time t, K is the number of observation angle pairs; X (SM_p and Z_p^S) are soil parameters to be retrieved.

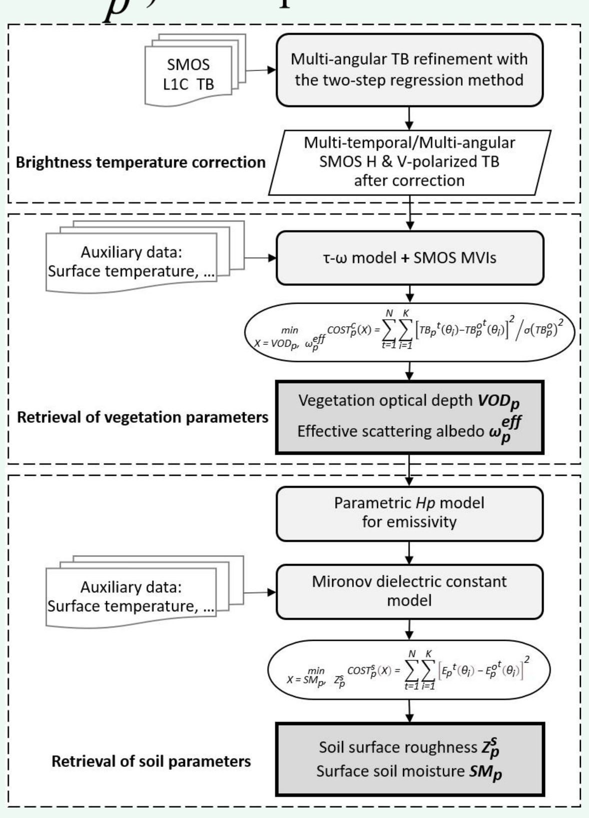

Fig.1. Flow chart of the MTMA method

3. Results and discussions

This paper for the first time at the global scale produced a polarization-dependent SMOS VOD_p and ω_p^{eff} products (**Fig.2 and Fig.3**), and their global spatial patterns follow global vegetation distributions, moreover, the preliminary exploration of the difference between H-pol and V-pol VOD_p and ω_p^{eff} may indicate that the vegetation effects can be polarization dependent even at large scales for satellite observations; the retrieved surface roughness (Z_p^S) range from 0.04 to 0.22 cm, and its spatial distribution is partially different from the existing roughness products/auxiliary data from SMOS and SMAP (Soil Moisture Active Passive) (**Fig.4**), moreover, this study discussed that the dependence of roughness effects on soil moisture still exists at satellite scales and can be explained by an exponential function for those sites where the retrieved roughness parameter changes over time; the spatial distribution of $MTMA-SM_p$ and SMOS products is generally consistent and reflects the spatial variations of SM in different climatic regions (**Fig.5**). The retrieved MTMA SM shows generally high correlations with in-situ measurements (11 dense observation networks) with overall correlation coefficients of more than 0.75 (**Fig.6**). The overall ubRMSE of $MTMA-SM_H$ and $MTMA-SM_V$ are less than 0.055 m³/m³ and lower than that of SMOS-IC and SMOS-L3 products. Therefore, it is concluded that by incorporating multi-temporal SMOS data, the proposed method of MTMA can be used to systematically retrieve SM, VOD and additional surface parameters (effective scattering albedo and surface roughness were retrieved in addition in this study) with comparable or better performance of SM than that of SMOS-IC and SMOS-L3.

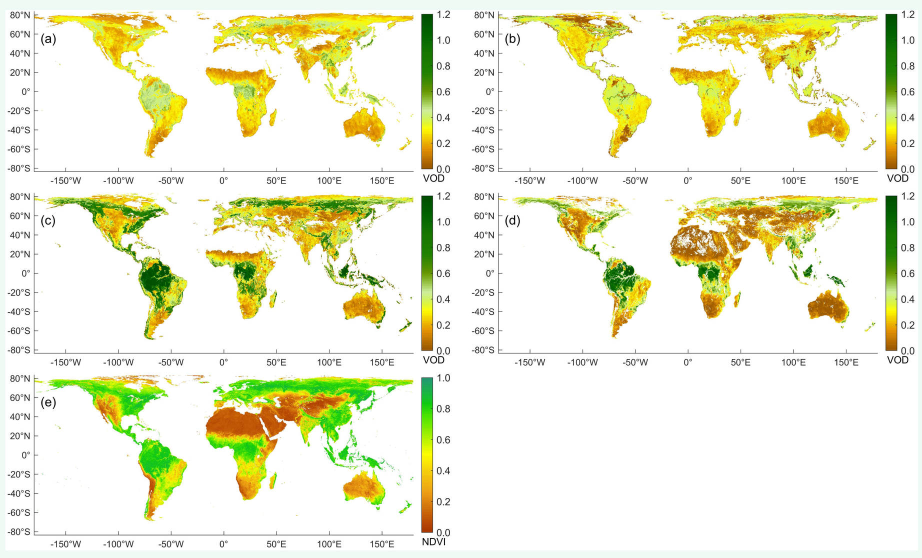

Fig.2. Global distribution of the monthly-averaged VOD in June 2017: (a) $MTMA-VOD_H$, (b) $MTMA-VOD_V$, (c) SMOS-L3 VOD at nadir, (d) SMOS-IC VOD, and (e) NDVI (MODIS).

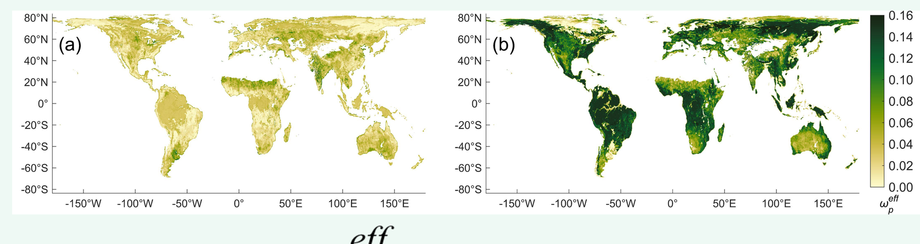

Fig.3. Retrievals of ω_p^{eff} based on SMOS multi-angular TB data in June 2017: (a) $MTMA-\omega_H^{eff}$ and (b) $MTMA-\omega_V^{eff}$.

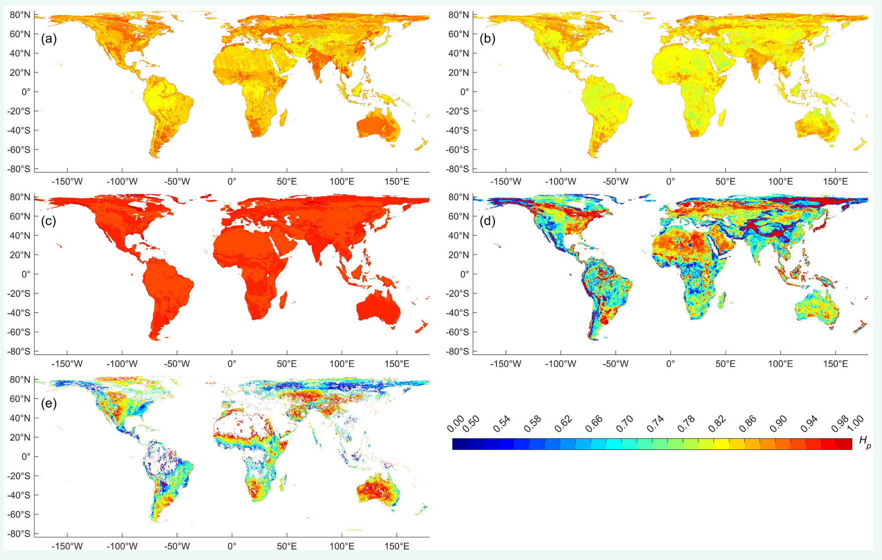

Fig.4. Global distribution of the time-averaged H_p: (a) the MTMA-H_H obtained using retrievals of Z_H^S by our method with H-pol TB, (b) the MTMA-H_V obtained using retrievals of Z_V^S by our method with V-pol TB, (c) the H_p obtained using soil roughness h of SMAP single channel algorithm (SCA) ancillary data, (d) the H_p obtained using soil roughness h of of SMAP dual channel algorithm (DCA) ancillary data and (e) the H_p obtained using soil roughness h estimated by SMOS data.

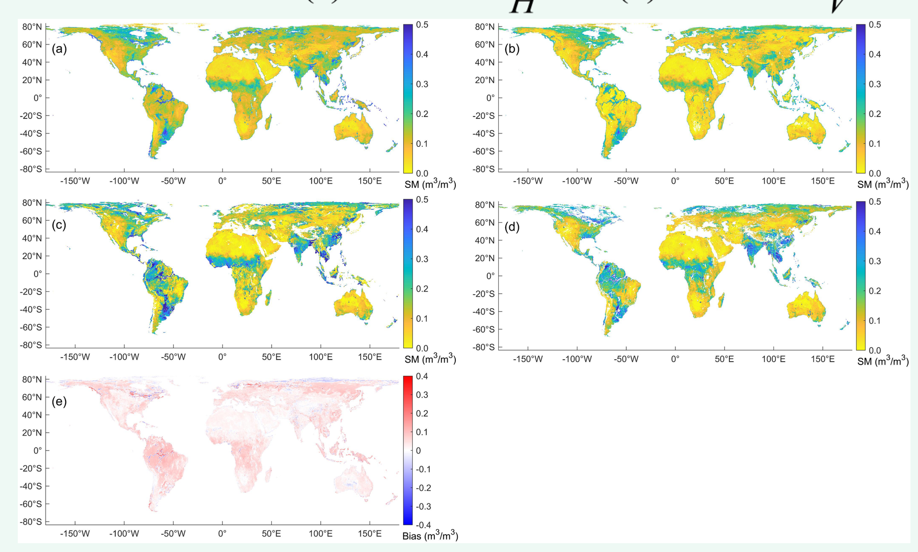

Fig.5. Global distribution of the time-averaged SM (sm³/sm³) in June 2017: (a) $MTMA-SM_H$, (b) $MTMA-SM_V$, (c) SMOS-L3 SM, (d) SMOS-IC SM and (e) the difference ($MTMA-SM_H$ minus $MTMA-SM_V$) between $MTMA-SM_H$ and $MTMA-SM_V$.

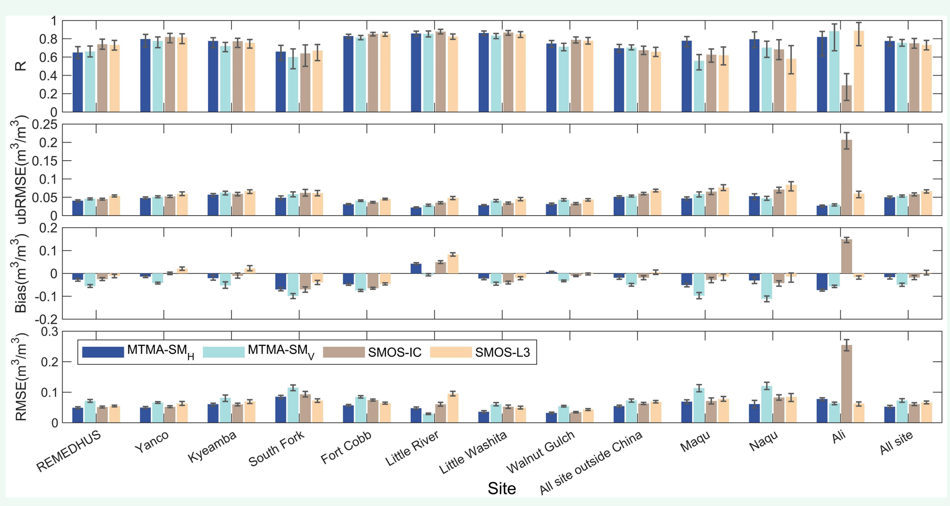

Fig.6. The performance metrics with 95% confidence intervals for SM retrievals at validation sites

4. outlook

In this study, we proposed a multi-temporal multi-angular (namely MTMA) approach to systematically retrieve four parameters of VOD_p, ω_p^{eff}, SM_p and Z_p^S based on the theory microwave vegetation indices from H-pol or V-pol SMOS data. The proposed algorithm assumes that vegetation parameters of VOD_p and ω_p^{eff} do not change in temporal adjacent overpasses, while soil parameters of SM_p and Z_p^S remain to be time-varying. The method proposed in this study takes full advantage of the multi-angular features of SMOS data to decouple the soil-vegetation interactions and makes full use of multi-temporal observations to increase the degree of information of satellite measurements used in the algorithm for additional retrieval of vegetation effective scattering albedo and soil roughness. The limitation of the algorithm is its great sensitivity to TB variability with incidence angles, resulting in increased uncertainties in dense vegetation areas (AGB above 200 Mg/ha), which should be further improved in subsequent research.

Acknowledgements

This study was jointly supported by the Strategic Priority Research Program of the Chinese Academy of Sciences (Grant No. XDA19030203), the Second Tibetan Plateau Scientific Expedition and Research Program (STEP) (Grant No. 2019QZKK0103, 2019QZKK0206) and the National Natural Science Foundation of China (NSFC) (Grant no. 42090014). We gratefully thank the Centre Aval de Traitement des Données SMOS and NASA Distributed Active Archive Center for providing satellite products. In-situ SM data are contributed partly by the International Soil Moisture Network (ISMN) and partly by the U.S. Department of Agriculture, Agricultural Research Service.

References

Cui, Q., Shi, J., Du, J., Zhao, T., Xiong, C., 2015. An Approach for Monitoring Global Vegetation Based on Multi-angular Observations From SMOS. IEEE Journal of Selected Topics in Applied Earth Observations and Remote Sensing, 8, 604-616.

Kerr, Y.H., Waldteufel, P., Wigneron, J.P., Martinuzzi, J., Font, J., Berger, M., 2001. Soil moisture retrieval from space: the Soil Moisture and Ocean Salinity (SMOS) mission. IEEE Transactions on Geoscience and Remote Sensing on Geoscience and Remote Sensing, 39, 1729-1735.

Konings, A.G., Piles, M., Rötzer, K., McColl, K.A., Chan, S.K., Entekhabi, D., 2016. Vegetation optical depth and scattering albedo retrieval using time series of dual-polarized L-band radiometer observations. Remote Sensing of Environment, 172, 178-189.

Konings, A.G., Piles, M., Das, N., Entekhabi, D., 2017. L-band vegetation optical depth and effective scattering albedo estimation from SMAP. Remote Sensing of Environment, 198, 460-470.

Shi, J., Jackson, T., Tao, J., Du, J., Bindlish, R., Lu, L., Chen, K.S., 2008. Microwave vegetation indices for short vegetation covers from satellite passive microwave sensor AMSR-E. Remote Sensing of Environment, 112, 4285-4300.

Shi, J., Zhao, T., Cui, Q., Yao, P., 2019. Airborne and Spaceborne Passive Microwave Measurements of Soil Moisture, 2, 71-105.

Zhao, T., Shi, J., Bindlish, R., Jackson, T.J., Kerr, Y.H., Cosh, M.H., Cui, Q., Li, Y., Xiong, C., Che, T., 2015. Refinement of SMOS Multiangular Brightness Temperature Toward Soil Moisture Retrieval and Its Analysis Over Reference Targets. IEEE Journal of Selected Topics in Applied Earth Observations and Remote Sensing, 8, 589-603.